NASA Technical Memorandum 86936

NASA-TM-86936 19850011959

Flow Visualization Study of the Effect of Injection Hole Geometry on an Inclined Jet in Crossflow

Frederick F. Simon and Michael L. Ciancone
Lewis Research Center
Cleveland, Ohio

Prepared for the
Symposium on Transport Phenomena in Rotating Machinery
cosponsored by the University of Michigan, University of Hawaii,
American Society of Mechanical Engineers, Gas Turbine Society of Japan,
Turbomachinery Society of Japan, and others
Honolulu, Hawaii, April 28–May 3, 1985

NASA

FLOW VISUALIZATION STUDY OF THE EFFECT OF INJECTION HOLE GEOMETRY ON AN INCLINED JET IN CROSSFLOW

Frederick F. Simon and Michael L. Ciancone
National Aeronautics and Space Administration
Lewis Research Center
Cleveland, Ohio 44135

SUMMARY

A flow visualization study using neutrally buoyant, helium-filled soap bubbles was conducted to determine the effect of injection hole geometry on the trajectory of an air jet in a crossflow and to investigate the mechanisms involved in jet deflection. Experimental variables were the blowing rate (M = 0.53, 1.1, 1.6, 4.1, and 6.2) and the injection hole geometry (cusp facing upstream (CUS), cusp facing downstream (CDS), round, swirl passage, and oblong). Results indicate that jet deflection is governed by both the pressure drag forces and the entrainment of free-stream fluid into the jet flow. The effect of the pressure drag force is that a jet presenting a larger projected area to the crossflow will be deflected initially to a greater extent. Thus for injection hole geometries with similar cross-sectional areas and similar mass flow rates, the jet configuration with the larger aspect ratio (major axis perpendicular to the crossflow) experienced a greater deflection. Entrainment arises as a result of lateral shearing forces on the sides of the jet, which set up a dual vortex motion within the jet and thereby cause some of the main-stream fluid momentum to be swept into the jet flow. This additional momentum forces the jet nearer the surface. Of the jet configurations examined in this study, the oblong, CDS, and CUS configurations exhibited the largest deflections. These results correlate well with film cooling effectiveness data, suggesting the need to determine the jet exit configuration of optimum aspect ratio to provide maximum film cooling effectiveness.

E-2450

SYMBOLS

A	cross-sectional area
C_d	flow discharge coefficient
D	effective diameter of jet at exit
g_c	Newton's constant
M	blowing rate, $(\rho U)_j/(\rho U)_\infty$
m	mass flow rate
P	static pressure
R	ratio of jet to main-stream velocity
Re	Reynolds number

T temperature

U velocity

X axial distance from downstream edge of jet exit

X/D dimensionless distance based on effective jet diameter at exit

Y vertical distance from wall

Y/D dimensionless vertical distance based on effective jet diameter at exit

η adiabatic film cooling effectiveness, $(T_\infty - T_{aw})/T_\infty - T_j)$

ρ density

Subscripts:

aw adiabatic wall

c centerline

j jet

L lower jet boundary

p plenum

∞ tunnel air, crossflow or free stream

INTRODUCTION

A jet in crossflow is of great practical significance for many engineering applications. The ratio of the jet mass flux to the main-stream mass flux (the blowing rate M) determines to a great extent the application to be considered. Applications range from the film cooling of turbine blades and the injection of jets into combusters to the transition flight of V/STOL aircraft or the disposal of wastes into the atmosphere. In dealing with these phenomena, it is important to know the flow field or jet trajectory that results from a given value of M. Although the results reported herein have general application, the motivation for the present study was the need to maintain a coolant film (film cooling) as close as possible to the surface of turbine blades exposed to high-temperature gases.

Papell (ref. 1) compares the film cooling efficiencies of a jet emanating from either a cusp-shaped hole or a standard discrete round hole into a crossflow for a range of blowing rates ($0.2 \leq M \leq 2.05$) and an injection angle of 30°. His visual evidence indicates that the cusp-shaped hole has a higher film cooling efficiency because its lower coolant jet trajectory deflects closer to the surface than the trajectory from a round hole at comparable conditions. Papell further postulates that the cusp-shaped hole produces a secondary flow consisting of a pair of counterrotating vortices that enhances the deflection of the jet trajectory. He supports this concept by using neutrally

buoyant helium-filled bubbles to delineate the jet flow region. Papell thus establishes the advantage of some noncircular holes in film cooling and hence the need for a greater understanding of the mechanisms involved in determining the trajectory of a jet in crossflow.

There is an abundance of information on jet trajectories for round injection holes (refs. 2 and 3) but little information for noncircular holes. Reference 2 alone contains 24 references of experimental investigations of round holes in crossflow. Reference 4 reports on the penetration of air jets from circular, square, and elliptical orifices at a known distance from the orifice. The long axis of the elliptical orifice was placed parallel to the crossflow. Reference 5 studies the temperature profile in the dilution zone of a combustion chamber created by jets flowing from "bluff"-shaped[1] slots and slots or orifices of other shapes. References 6 and 7 investigated the effect of a normal jet on the pressure distribution on a flat surface with round- and oblong-shaped injection holes (crossflow parallel and perpendicular to major axis). References 5 and 6 provide some general information on the effect of orifice configuration on jet flow but no detailed information on jet trajectories. Rather than focusing on film cooling effectiveness, the present study goes beyond the preliminary flow visualization results of reference 1 and attempts to develop a sound relationship by providing experimental jet trajectory data for circular and noncircular holes for several values of M.

Previously it had been demonstrated that greater film cooling efficiency could be obtained by using a curved-tube inlet channel (ref. 8), "shaped" holes (ref. 9) (which decrease the jet momentum and employ the Coanda effect[2] to decrease the penetration of the coolant jet into the main stream), and compound-angle injection (ref. 10) (to keep the jet attached to the surface). An analysis of the existing literature on jet trajectories indicates three general categories of jet/crossflow interactive mechanisms:

(1) Only entrainment of the free stream by the jet governs the interaction (refs. 11 to 13).

(2) Only pressure forces acting on the jet govern the interaction (ref. 14).

(3) Both entrainment and pressure forces are considered in the interaction (refs. 15 to 20).

From these studies it became apparent that an understanding of the interaction between the jet and the crossflow is crucial to determining the trajectory of the deflected jet.

A jet, in terms of its history as it penetrates into the main stream, can be described in terms of three regions: (1) the potential core region, region I; (2) the developed turbulent flow region, region II; and (3) the far downstream region, region III.

---

[1]Oblong-shaped orifice with long axis perpendicular to crossflow.

[2]Henri Coanda (1932) observed that a free jet emerging from a nozzle will follow a nearby curved or inclined surface or will come in contact with the surface. This effect is caused by jet stream entrainment, which creates a partial vacuum.

In region I, the fluid jet penetrating the crossflow forms a potential core of essentially constant velocity. This retards the main stream along the upstream side of the jet and increases the pressure. On the downstream side of the jet a rarefaction, or wake region, occurs. Coupled with the upstream pressure, it produces a pressure differential that deflects the jet toward the surface. Kamotani's (ref. 21) experimental results indicate that this deflection begins very close to the jet exit. Platten (ref. 22) found that for low values of the ratio of jet to main-stream velocity R the deflection of the potential core by the pressure gradient normal to the jet begins to become appreciable.

Viscous entrainment of the main-stream fluid denotes the beginning of the developed turbulent flow region (region II, approximately three diameters downstream). Lateral shearing action sweeps main-stream fluid around the sides of the jet and into the central jet region via entrainment through the underside of the jet. The overall effect is the creation of a counterrotating pair of vortices within the jet that tend to deform the jet cross section into a kidney shape (fig. 1). This secondary motion enhances the entrainment of the main-stream fluid, along with its corresponding momentum, into the jet. This further deflects the jet toward the surface. In addition, as the jet proceeds downstream, the kidney-shaped cross section presents a greater drag surface to the main stream, thereby enhancing the deflection due to pressure forces. Reference 23 suggests that this secondary vortex motion is influenced by the velocity profile within the jet flow passage and that it may be possible to enhance the secondary motion caused by the interaction of the jet and the main stream by changing the shape of the passage. In the developed turbulent flow region (region II) jet deflection is due to both the entrainment of mainstream fluid and the pressure forces induced by the main stream interacting with the jet.

Figure 61 of reference 13 shows that for a ratio of jet length to diameter greater than approximately 18 the effects of main-stream entrainment dominate the jet trajectory. This is the far downstream region (region III), where pressure forces no longer play a significant role in determining the jet trajectory.

In the present work jet trajectories were photographed for five injection hole geometries at blowing rates M of 0.53, 1.1, 1.6, 4.1, and 6.2 for a jet injection angle of 30° with respect to the upstream horizontal. Relevant data were extracted from these photographs and used in a comparative analysis of the effect of injection hole geometry on jet trajectory to assess the mechanisms contributing to jet deflection.

APPARATUS

The flow visualization test rig (fig. 2) consisted of a transparent plastic tunnel through which air was drawn into a vacuum exhaust line. This simple construction provided flexibility for testing a large number of injection hole geometries appropriate to turbine and combustor cooling applications. The test configuration for this report consisted of a zero-pressure-gradient, free-stream flow over a flat surface containing an injection hole. The tunnel section containing the test plate was positioned so that there was about 1.3 m of tunnel length (not including contoured inlet) upstream of the jet exhaust. Thus at the point of jet exit the injection surface boundary layer was fully

turbulent as determined in a previous investigation with this tunnel (ref. 8). The three separate ambient airflow sources were the primary free-stream airflow, the bubble generator airflow, and the secondary jet air (fig. 3).

The jet air was supplied to the plenum by means of a Hilsch tube connected to a 827-kPa (120-psi) dry air source. This source, which incorporated a vortex generator element, separated the inlet air into hot and cold streams. This separation resulted from the forced vortex, or wheel, type of angular velocity imparted to the air entering the device. Conservation of the total energy of the inner region of the contained vortex caused heat to be transferred to the outer region of the vortex. Consequently a relatively cold inner core of air and a warm outer ring of air were available. In the Hilsch tube design the warm and cold air discharge ports are on opposite ends of the tube. Cold-end temperatures of 0 °C were available with this device, so some variation in the jet density was possible.

The tunnel air temperature was measured with a thermocouple mounted in the contoured inlet. The coolant air temperature was measured with a thermocouple mounted in the plenum between the screens and the mahogany test plate. The coolant airflow rate was measured with a turbine type of flowmeter installed between the Hilsch tube and the coolant plenum. The tunnel velocity was determined from pitot-static pressure readings taken upstream of the test section.

The bubble generator system employed in the present study was used in the visual study of reference 10 and consisted of a head (which formed the bubbles) and a console (which controlled the flow of helium, bubble solution, and air to the head). A drawing illustrating the basic features of the head is shown in figure 4. Neutrally buoyant, helium-filled bubbles, about 1 mm in diameter, formed on the tip of the concentric tubes and were blown off the tip by air flowing through the shroud passage. Bubble solution flowed through the annular passage and was formed into bubbles at the tip. These bubbles were inflated with helium passing through the inner concentric tube. The desired bubble size and neutral buoyancy were achieved by proper adjustment of air, bubble solution, and helium flow rates. For this study a setting was established to produce the largest number of bubbles possible that were small enough to survive passage through the plenum and the jet exit channel. As many as 300 bubbles per second can be formed by this device.

The neutrally buoyant, helium-filled bubbles were injected into a plenum, which served as a collection chamber for the bubbles and the jet air. The air, seeded with the bubbles, then passed through the jet passage and into the test region. The small quantity of air used by the bubble generator to blow the bubbles off the tip of the annulus as they formed ended up as part of the jet air in the plenum. Consequently the mass contribution of the bubble generator was measured by a rotameter. This small, but not negligible, correction to the jet mass flow was subsequently accounted for in calculating the blowing rate M. The plenum box was clamped onto the bottom of the test section for easy removal when another test plate with a different injection hole geometry was to be tested. The configurations were cast in epoxy as inserts to be installed in the flat plate. Schematic drawings of the cross-sectional areas of the various configurations investigated are displayed in figure 5.

The 0.38- by 0.61-m floor of the test section, which contained the jet injection hole, was easily removable to allow bottom plates with different hole

configurations to be installed without affecting the rest of the test section or the plenum chamber. The jet flow passage length of 6.35 cm provided a ratio of jet flow passage length to diameter of 5.0 (typical of aircraft turbine applications). All configurations had an equivalent diameter of 1.27 cm based on a constant cross-sectional area of 5.07 cm^2 to allow the mass flow rate to be independent of jet configuration. The floor and back side of the test section were made of wood and had a glossy black finish to give maximum contrast with the bubble streaklines.

A high-efficiency 300-W xenon quartz arc lamp provided sufficient light intensity for photographing the bubbles (fig. 6). A metal plate with a rectangular slot cutout was placed between the light source and the lens to shape the light beam, and an infrared reflecting filter was used to prevent heating of bubbles passing through the beam. The beam was then focused through a 300-mm lens to form a sharply defined rectangular pattern of collimated light (7.7 by 15.2 cm) through which the bubbles passed as they exited the jet flow passage.

EXPERIMENTAL PROCEDURE

Typical test procedure consisted of filming the test section from the lower surface level for a variety of injection hole geometries and blowing rates as the bubble-delineated jet flow interacted with the free stream. Upon their passage through the jet exit channel and entrance into the test section, the bubbles contained within the jet flow were illuminated by the light beam emitted by a high-intensity xenon arc lamp situated upstream of the flow and directed parallel to the free stream.

As the soap bubbles passed through the illuminated region of the test section, their movement was recorded on film as a series of streaklines caused by light reflecting from the surface of the bubbles as they passed through the illuminated portion of the photographic field. A sequence of photographs exposed for different times was produced to achieve the optimum setting for each set of test conditions. Too few streaklines would result in a photograph lacking definition; too many streaklines would tend to wash out the entire frame. Generally speaking exposure times ranged from 20 to 80 sec at an aperture setting of f5.6 for a film speed of ASA 400.

This attention to exposure time was a direct result of the need for a statistically significant number of streaklines in each photograph, in addition to the desire for quality flow visualization. Assuming the bubbles would faithfully and accurately follow the jet flow as it entered the test region and mixed with the free stream, this nonetheless dictated the statistical nature of the bubble movement as a function of each bubble's departure point from the jet orifice - hence the randomness associated with each streakline location. It was desirable to establish a large number of streaklines in each photograph to ensure that the jet region was delineated realistically as it began to mix, and eventually merge, with the free stream. This procedure provided sufficient data to identify the effect of hole geometry on jet trajectory in a crossflow.

The high and low extents of the jet flow region were identified in each photograph at axial downstream distances X/D of 0.5, 1.0, 1.5, 2.0, 3.0, 4.0, 5.0, 8.0, 10.0, and 12.0. From these, the jet centerline height was calculated by averaging the values of the high and low vertical positions of the

jet boundary. Measured data were stored in a data set to be graphically output via the ZETA12 graphics capabilities of the IBM 370 computer system.

RESULTS AND DISCUSSION

Figures 7 and 8 represent the jet trajectory centerline data and the lower jet boundary data for the five injection hole geometries investigated in this study. Representative values of blowing rate M and density ratio ρ_j/ρ_∞ are indicated in each figure. Abramovich's empirical prediction (ref. 24) based on round holes is included as a basis for comparison with the jet centerline data. There is general agreement with the round-hole data. In general, the round hole with a swirl passage insert produced the highest jet trajectory. The cusp facing upstream (CUS), cusp facing downstream (CDS), and oblong holes produced the lowest trajectories. The lowering of the jet trajectory by an oblong hole is also suggested by the temperature profile results of reference 5 and by the limited jet trajectory information of reference 6. Photographs of jets are shown in figure 9.

According to reference 25, the use of a swirl tape insert (fig. 5(b)) should markedly increase the entrainment of main-stream fluid into the jet. In the present experiments the spreading rate of the jet produced by the swirl configuration was greater than those of the other configurations, an indication that entrainment would also be greater for the swirl configuration. It had been expected that the additional entrainment of main-stream fluid would effectively increase jet deflection toward the surface. However, inasmuch as this was not the case in the present study, it was conjectured that the swirl component of jet velocity diminished the effect of drag and entrainment on the jet centerline trajectory. The swirl-produced jet (fig. 9) appeared relatively unaffected by the main-stream flow to an axial distance of several diameters downstream of the jet exit. Apparently the main-stream fluid entrained by the jet lost some of its axial momentum to the swirl component of the jet. In addition, the small effect of pressure drag forces on jet trajectory in the potential core region was probably due to the swirl component of the jet preventing the crossflow shearing action across the jet, which would otherwise set up the pressure differential necessary to deflect the jet. This is analogous to the method given in reference 26 for reducing pressure drag through the use of a moving surface that effectively reduces the relative velocity at the shear interface. Therefore it appears that in the case of the swirl configuration, decreased drag and decreased axial momentum combined to produce a jet that was deflected least among the configurations within the scope of this study.

Figure 10 points out the effect of the initial jet cross section on pressure drag, and hence on the deflection trajectory, by comparing the deflection trajectories for round and oblong holes. The oblong hole produces an initial jet shape that has a drag coefficient at least twice that of the round hole. The effect that increased pressure drag can have on jet trajectory, namely a greater deflection of the jet, is illustrated in figure 10 for blow rates M of 1.6 and 0.5 for the analysis of reference 14 and the data of the present experiments. The analysis of reference 14, which predicts jet centerline trajectory based solely on drag, is insufficient to describe the jet centerline trajectory. Because of the lack of difference in entrainment for M of 1.6 and 0.5 (based on inspection of jet expansion) for both the round and oblong holes, the difference in jet trajectories observed in figure 10 was assumed to be a function of pressure drag only. The difference in the experimental curves

would be slightly greater if the projected area diameter (D = 1.98 cm) were used for the oblong hole. The use of a projected area diameter is consistent with the drag analysis of reference 14. This difference is also seen in the theoretical curves of figure 10. An example of how drag plays a key role in determining jet trajectory is provided by injecting jets at angles lateral to the direction of the main stream as a means of increasing film cooling efficiency by forcing the jet nearer to the surface (ref. 10). A jet that attempts to laterally penetrate the main stream presents a much greater projected area to the main-stream flow than an aligned jet with an aspect ratio that increases with lateral angle. The greater projected area results in increased pressure drag. This pressure drag and the accompanying entrainment of main-stream fluid into the jet keeps the jet flow near the surface.

From a comparison of the experimental and theoretical curves of figure 10, it appears that entrainment begins to play a major role in determining the jet trajectory at relatively small axial downstream distances. This is consistent with the length of the potential core region (region I) being only of the order of one diameter at low values of M. It is expected that greater drag in region I will increase both the drag and the entrainment of main-stream fluid into the jet in region II. This additional entrainment of fluid should deflect the jet closer to the wall.

For all the blowing rates considered, the jet produced by the CDS configuration generally exhibited a larger deflection than that produced by the CUS configuration. This suggested that the jet surface facing the cross stream had higher pressure drag properties for the CDS configuration than for the CUS configuration. Some confirmation of this is suggested by the measurements of jet flow discharge coefficients.

The jet flow discharge coefficient, which is a measure of the jet frictional losses, is defined as follows:

$$C_d = U_j \Big/ \sqrt{\frac{2g_c(P_p - P_\infty)}{\rho_j}} \tag{1}$$

where

$$U_j = m_j / \rho_j A_j$$

The discharge coefficient is plotted as a function of the jet Reynolds number based on hydraulic diameter in figure 11 for the round, CUS, and CDS injection hole geometries. Discharge coefficients were measured by exhausting a jet into a relatively slow-moving cross stream so as to minimize the entrainment effect of free-stream axial momentum and thus leave a relative measure of frictional losses. Since the same test section was used for both CUS and CDS hole configurations, a difference in discharge coefficient could not be expected on the basis of frictional losses incurred within the jet channel. However, equation (1) states that the discharge pressure is the free-stream pressure; therefore the flow coefficient includes frictional losses created by the jet-crossflow interaction, which could differ between the injection hole geometries in question. It was expected from jet trajectory curves that the CDS hole would produce the highest frictional loss and the lowest discharge coefficient since it produces a higher pressure drag. The results of figure 11 support this assumption.

The aspect ratios were 2.78 for the oblong hole and 2.0 for the CUS and CDS holes. It was inferred from this difference that the aspect ratio of a jet injection hole is important in determining the jet trajectory, particularly when drag forces dominate. However, as indicated in reference 23, the jet velocity profile is also of importance. The differences in velocity profile produced by the CUS and oblong holes may account for the respective differences in jet trajectories. Papell (refs. 1 and 8) postulates that the production of secondary flows in the jet before its injection into the free stream will result in greater deflection of the jet toward the wall. Although the effects of secondary motions or velocity profiles were not considered in this study, there is a need for these effects to be studied in the future.

FILM COOLING APPLICATION

Since the same facility and some of the same jet injection hole geometries (CUS, CDS, and round) were used in this study and in Papell's investigation (ref. 1), it was of interest to compare the jet deflection trajectory data of this study with the film cooling effectiveness data of reference 1. Some of these data are reproduced in figure 12. Although the jet centerline data of figure 7 give some correlation with film cooling effectiveness, a better correlation is obtained by using the height of the lower jet boundary as a function of axial distance downstream X/D (fig. 8).

Figure 13 shows that a general relationship exists between the film cooling effectiveness (from fig. 12) and the height of the lower jet boundary Y_L (figs. 8(a), (c), and (d)). This set of curves illustrates, as expected, that as Y_L decreased, film cooling effectiveness increased. In addition, the film cooling effectiveness near the jet exit (X/D = 1, fig. 13(a)) is quite sensitive to the location of the jet with respect to the wall. Depending on the value of Y_L, the cooling of the downstream exit area is either efficient or relatively inefficient (fig. 13(c)). Based on the results of reference 27, this indicates little or no recirculation of main-stream fluid about the exit location as the jet touched or was very close to the wall. In the case of separation, inferred from larger values of Y_L, the jet turned toward the surface and reattached. Reattachment represents the maximum in film cooling effectiveness (fig. 12).

Comparing the film cooling effectiveness for M = 1.5 (fig. 12(c)) with Y_L at a blowing rate of M = 1.6 (fig. 8(d)) illustrates the correlation of heat transfer and jet location. At X/D = 1, the relative positions from figure 8(d) in decreasing order of vertical height are round, CUS, and CDS. This corresponds to the greater film cooling effectiveness shown in figure 12(c) for M = 1.5 and X/D = 1. Film cooling effectiveness increased in the order of round, CUS, and CDS. The order of film cooling effectiveness changed beyond X/D = 2 (fig. 12(c)), with the new order being round, CDS, and CUS. This change is reflected in the change in order of decreasing lower jet boundary Y_L beyond X/D = 4 of round, CDS, and CUS. Therefore the crossover in film cooling effectiveness (fig. 12(c), M = 1.5) appears to be supported by the visual evidence. At lower values of M (1.0 or 0.5), the jet trajectory data grouped quite closely together (and well within the level of experimental error). Hence a correspondence to the order of film cooling effectiveness is more difficult to determine.

The visual (fig. 9(b)) and heat transfer (fig. 12) evidence suggests that there is initially a greater turning of the jet toward the surface for the CDS configuration than for the CUS configuration. This turning is probably due to the greater pressure drag created by the CDS hole, as mentioned in our earlier discussion on jet centerline trajectory, and is best seen for the oblong hole (fig. 9). Drag near the jet exit has the additional effect of increasing the dual vortex motion and entrainment of the free-stream fluid into the jet (a further aid in deflecting the jet). This increased entrainment should decrease the coolant potential of the jet as noted in figure 12 at M of 1.0 and 1.5 for $X/D > 2$. In addition, the visual evidence of figure 9(b) for $M = 1.0$ indicates that after the jet reattaches to the wall it proceeds further and further from the surface. This effect was originally observed in the visual experiments of reference 26.

The lower jet boundary information (figs. 8(a), (c), and (d)) and the visual information (fig. 9) for the oblong hole suggests that it has a high potential for providing effective film cooling. If we use Y_L as a measure of film cooling effectiveness, the oblong hole should be as effective as both cusp holes. An additional factor to be considered is the amount of free-stream fluid entrained into the jet created by the oblong hole. Indeed, there is probably an optimum aspect ratio of such a hole since increasing the aspect ratio increases both drag and entrainment and the entrainment effectively diminishes the jet film cooling effectiveness. However, this increased jet dilution could be advantageous in combustor applications. For information on dilution jet experiments, refer to references 5 and 29.

The following are recommendations for future work:

(1) Experimentally determine the optimum aspect ratio for an oblong or elliptical jet injection hole that results in maximum film cooling effectiveness.

(2) Perform a general analysis of a jet in crossflow that takes into consideration the effects of jet cross section, jet velocity profile, and secondary flows on entrainment and on such jet characteristics as jet deflection and spreading, both horizontally and vertically.

CONCLUSIONS

Trajectory information was obtained for jet in a crossflow for five jet injection hole geometries at ratios of jet mass flux to main-stream mass flux (the blowing rate M) of 0.53, 1.1, 1.6, 4.1, and 6.2. From this information, the following conclusions were drawn:

(1) The nature and extent of pressure drag forces and the entrainment of freestream fluid into the jet play an important role in determining the extent of jet deflection toward the injection surface.

(2) Increasing the aspect ratio of the jet injection hole, with the long axis measured perpendicular to the main flow direction, increases jet deflection toward the injection surface.

(3) Visual evidence confirms that film cooling effectiveness increases with increasing deflection of the jet toward the injection surface.

REFERENCES

1. Papell, S.S., "Vortex Generating Flow Passage Design for Increased Film-Cooling Effectiveness and Surface Coverage," NASA TM-83617, 1984.

2. Crabb, D., Durao, D.F.G., and Whitelaw, J.H., "A Round Jet Normal to a Crossflow," ASME Journal of Fluids Engineering, Vol. 103, No. 1, Mar. 1981, pp. 142-153.

3. Margason, R.J., "The Path of a Jet Directed at Large Angles to a Subsonic Free Stream," NASA TN D-4919, 1968.

4. Ruggeri, R.S., Callaghan, E.E., and Bowden, D.T., "Penetration of Airjets Issuing from Circular, Square and Elliptical Orifices Directed Perpendicularly to an Air Stream," NACA TN-2019, 1950.

5. Holdeman, J.D., and Srinivasan, R., "Experiments in Dilution Jet Mixing - Effects of Multiple Rows and Non-Circular Orifices," AIAA/ASME/SAE 21st Joint Propulsion Conference, 8-11 July 1985, Monterey, CA.

6. McMahon, H.M. and Mosher, D.K., "Experimental Investigation of Pressures Induced on a Flat Plate by a Jet Issuing into a Subsonic Crosswind," Analysis of a Jet in a Subsonic Crosswind, NASA SP-218, 1969, pp. 49-62.

7. Wu, J.C. and Wright, M.A., "A Blockage-Sink Representation of Jet Interference Effects for Noncircular Jet Orifices," Analysis of a Jet in a Subsonic Crosswind, NASA SP-218, 1969, pp. 85-100.

8. Papell, S.S., Wang, C.R., and Graham, R.W., "Film-Cooling Effectiveness with Developing Coolant Flow Through Straight and Curved Tubular Passages," NASA TP-2062, 1982.

9. Goldstein, R.J., and Eckert, E.R.G., "Effects of Hole Geometry and Density on Three-Dimensional Film Cooling," International Journal of Heat and Mass Transfer, Vol. 17, No. 5, May 1974, pp. 595-607.

10. Colladay, R.S., and Russell, L.M., "Streakline Flow Visualization of Discrete-Hole Film Cooling with Normal, Slanted, and Compound Angle Injection," NASA TN D-8248, 1976.

11. Braun, G.W., and McAllister, J.D., "Cross Wind Effects on Trajectory and Cross Sections of Turbulent Jets," Analysis of a Jet in a Subsonic Crosswind, NASA SP-218, 1969, pp. 141-164.

12. Fearn, R,L., "Mass Entrainment of a Circular Jet in a Crossflow." Analysis of a Jet in a Subsonic Crosswind, NASA SP-218, 1969, pp. 239-248.

13. McAllister, J.D., "A Momentum Theory for the Effects of Cross Flow on Incompressible Turbulent Jets," Ph.D. Thesis, Univ. of Tennessee, Aug. 1968.

14. Hanus, G.J., and L'Ecuyer, M.R., "Turbine Vane Gas Film Cooling with Injection in the Leading Edge Region from a Single Row of Spanwise Angled Holes," TSPC TR-76-1, Purdue Univ., West Lafayette, IN, Apr. 1976, (NASA CR-147160).

15. Kamotani, Y., and Greber, I., "Experiment on a Turbulent Jet in Cross Flow," FTAS/TR-71-62, Case Western Reserve Univ., Cleveland, OH, June 1971, (NASA CR-72893).

16. Wooler, P.T., Burghart, G.H., and Gallagher, J.T., "Pressure Distribution on a Rectangular Wing with a Jet Exhausting Normally into an Airstream," Journal of Aircraft, Vol. 4, No. 6, Nov.-Dec. 1967, pp. 537-543.

17. Sucec, J., and Bowley, W.W., "Prediction of the Trajectory of a Turbulent Jet Injected into a Crossflowing Stream," ASME Journal of Fluids Engineering, Vol. 98, No. 4, Dec. 1976, pp. 667-673.

18. Adler, D., and Baron, A., "Prediction of a Three-Dimensional Circular Turbulent Jet in Crossflow," AIAA Journal, Vol. 17, No. 2, Feb. 1979, pp. 168-174.

19. Stoy, R.L., and Ben-Haim, Y., "Turbulent Jets in a Confined Crossflow," ASME Journal of Fluids Engineering, Vol. 95, No. 4, Dec. 1973, pp. 551-556.

20. Wang, C.R., Papell, S.S., and Graham, R.W., "Analysis for Predicting Adiabatic Wall Temperatures with Single Hole Coolant Injection into a Low Speed Crossflow," NASA TM-81620, 1981.

21. Kamotani, Y., and Greber, I., "Experiments on a Turbulent Jet in a Cross flow," AIAA Journal, Vol. 10, No. 11, Nov. 1972, pp. 1425-1429.

22. Platten, J.L., and Keffer, J.F., "Deflected Turbulent Jet Flows," ASME Journal of Applied Mechanics, Vol. 38, No. 4, Dec. 1971, pp. 756-758.

23. Gibeling, H.J., et al., "Computation of Discrete Slanted Hole Film Cooling Flow Using the Navier-Stokes Equations," R83-910002-F, Scientific Research Associates, Inc., Glastonbury, CT, Sept. 1983, (AFOSR-83-1288TR, AD-A137022).

24. Abramovich, G.N., The Theory of Turbulent Jets. MIT Press, Cambridge, MA, 1963.

25. Pratte, B.D., and Keffer, J.F., "Swirling Turbulent Jet Flows - Part 1: The Single Swirling Jet," UTME-TP-6901, Univ. of Toronto, Toronto, Canada, 1969.

26. Hoerner, S.F., Fluid-Dynamic Drag, Midland Park, NJ, 1965.

27. Bergeles, G., Gosman, A.D., and Launder, B.E., "Near-Field Character of a Jet Discharged Through a Wall at 30° to a Mainstream," AIAA Journal, Vol. 15, No. 4, Apr.1977, pp. 499-504.

28. Colladay, R.S., Russell, L.M., and Lane, J.M., "Streakline Flow Visualization of Discrete Hole Film Cooling with Holes Inclined 30° to Surface," NASA TN D-8175, 1976.

29. Holdeman, J.D., Srinivasan, R., and Berenfeld, A., "Experiments in Dilution Jet Mixing," AIAA Journal, Vol. 22, No. 10, Oct. 1984, pp. 1436-1443.

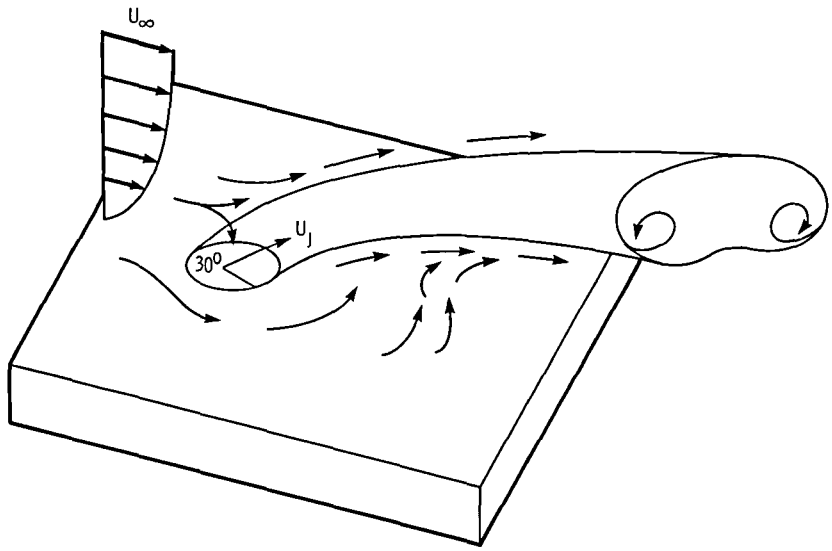

Figure 1 - Representations of a jet in crossflow

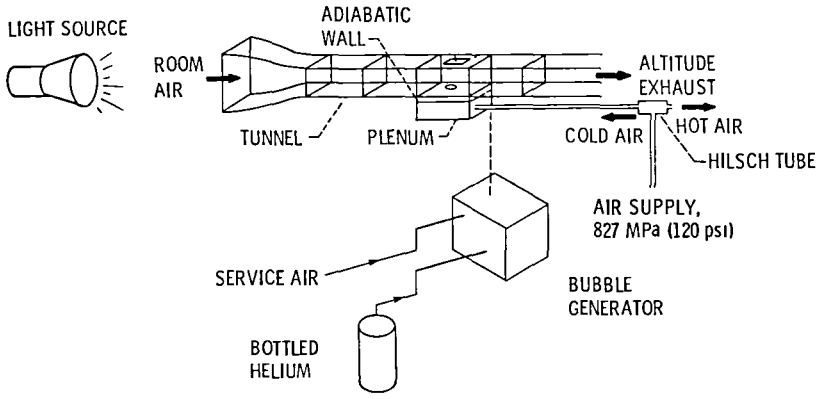

Figure 2. - Schematic of test plate and plenum air supply.

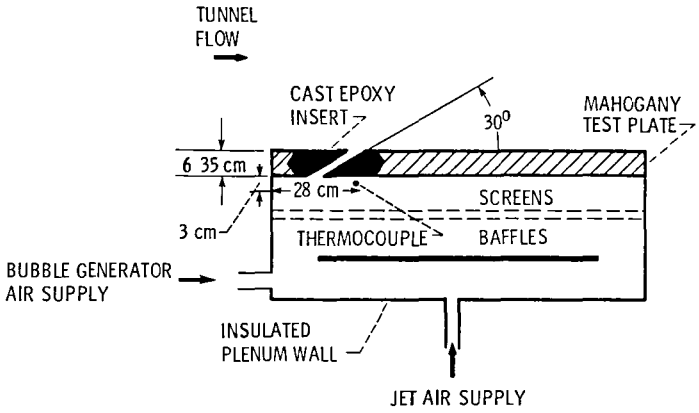

Figure 3 - Flow visualization rig.

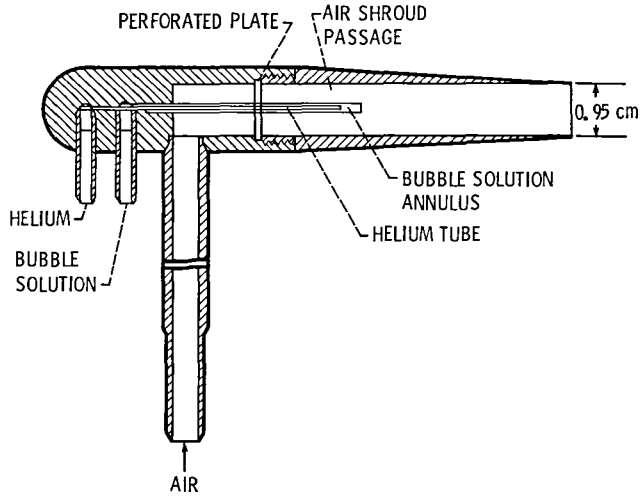

Figure 4 - Bubble generator head

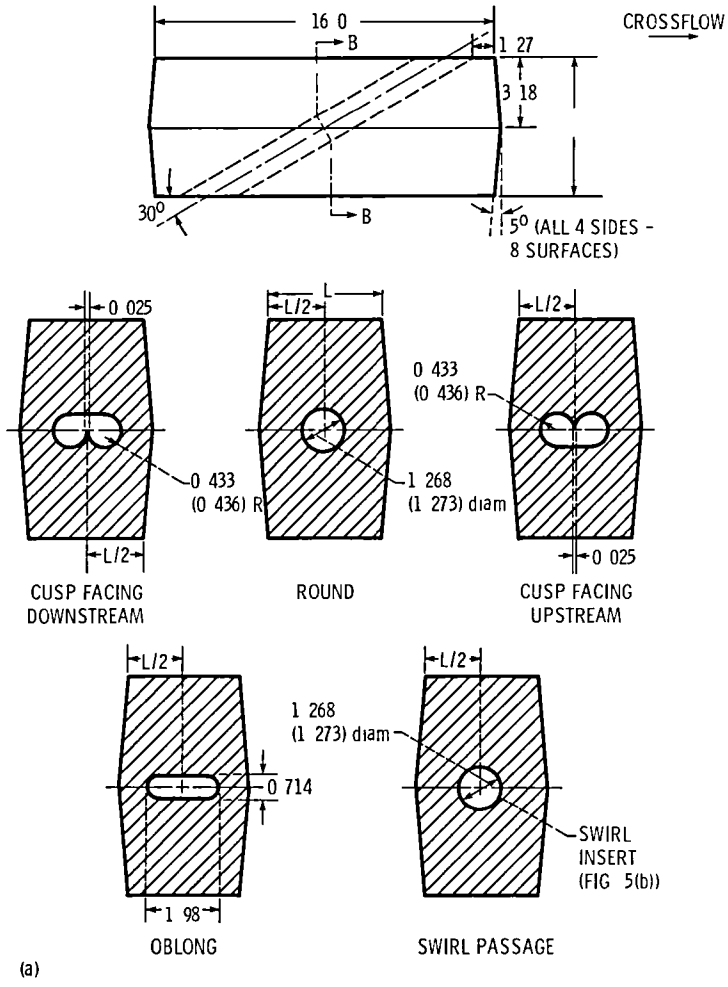

(a) Jet flow passage

(b) Swirl insert (twisted tape) for film cooling hole Twist is in clockwise direction when viewed from end of tape, Y is period of revolution (i e , distance over which a complete 360° twist is completed), t = 0 16 cm

Figure 5 - Geometry (Dimensions are in centimeters)

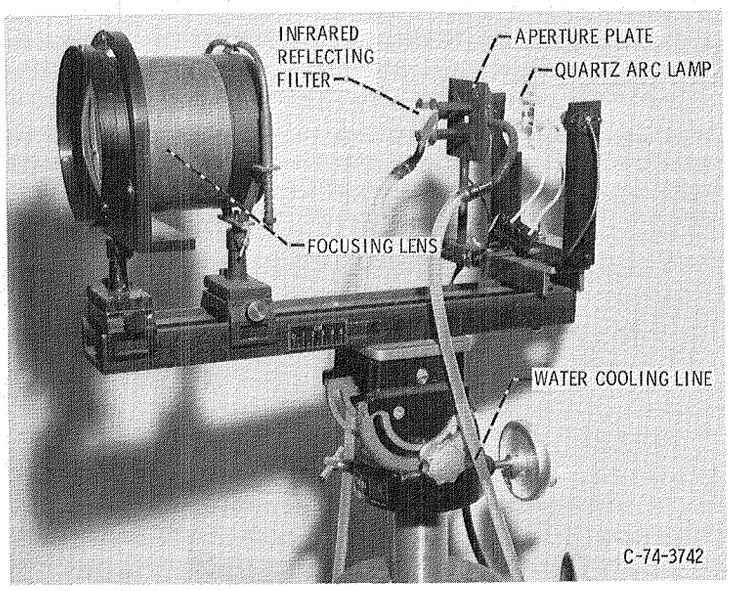

Figure 6. - Light source assembly.

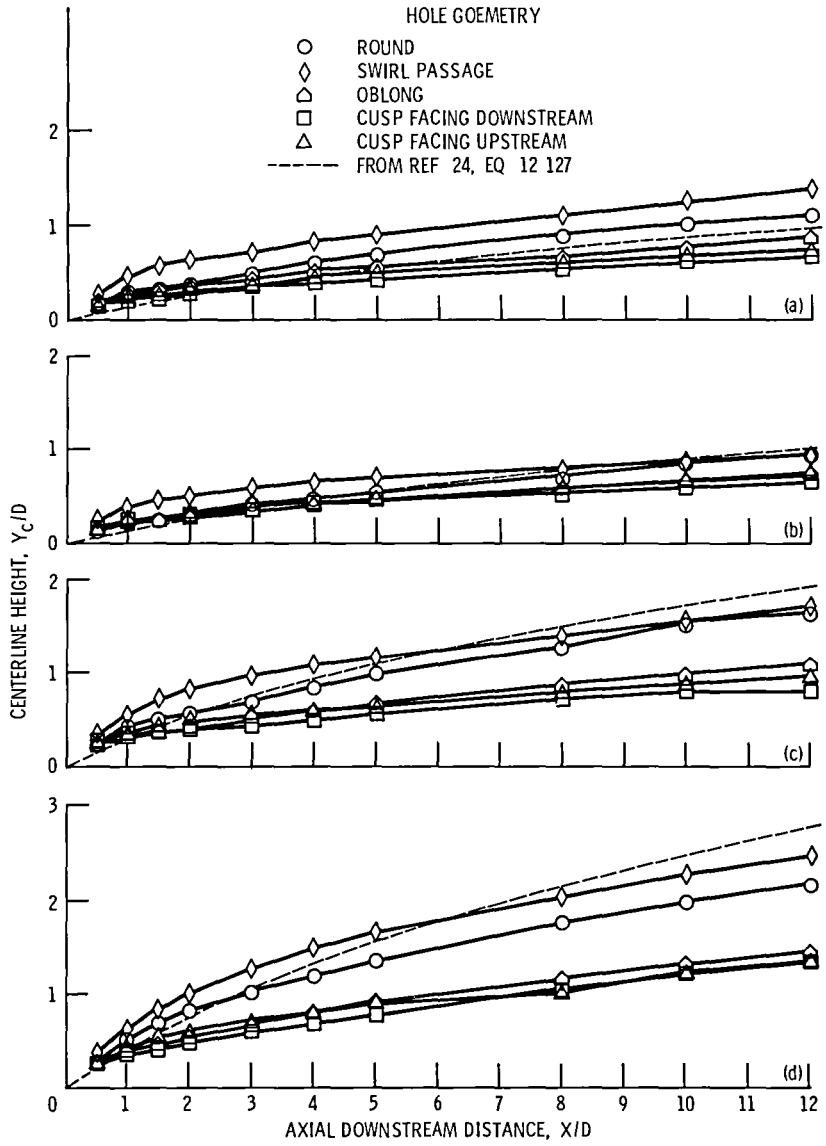

(a) $M = 0.53$, $\rho_j/\rho_\infty = 1.02$, $U_\infty = 16$ m/sec.
(b) $M = 0.53$, $\rho_j/\rho_\infty = 1.02$, $U_\infty = 31$ m/sec
(c) $M = 1.1$, $\rho_j/\rho_\infty = 1.03$, $U_\infty = 16$ m/sec.
(d) $M = 1.6$, $\rho_j/\rho_\infty = 1.04$, $U_\infty = 16$ m/sec.

Figure 7 - Jet centerline height as a function of axial distance.

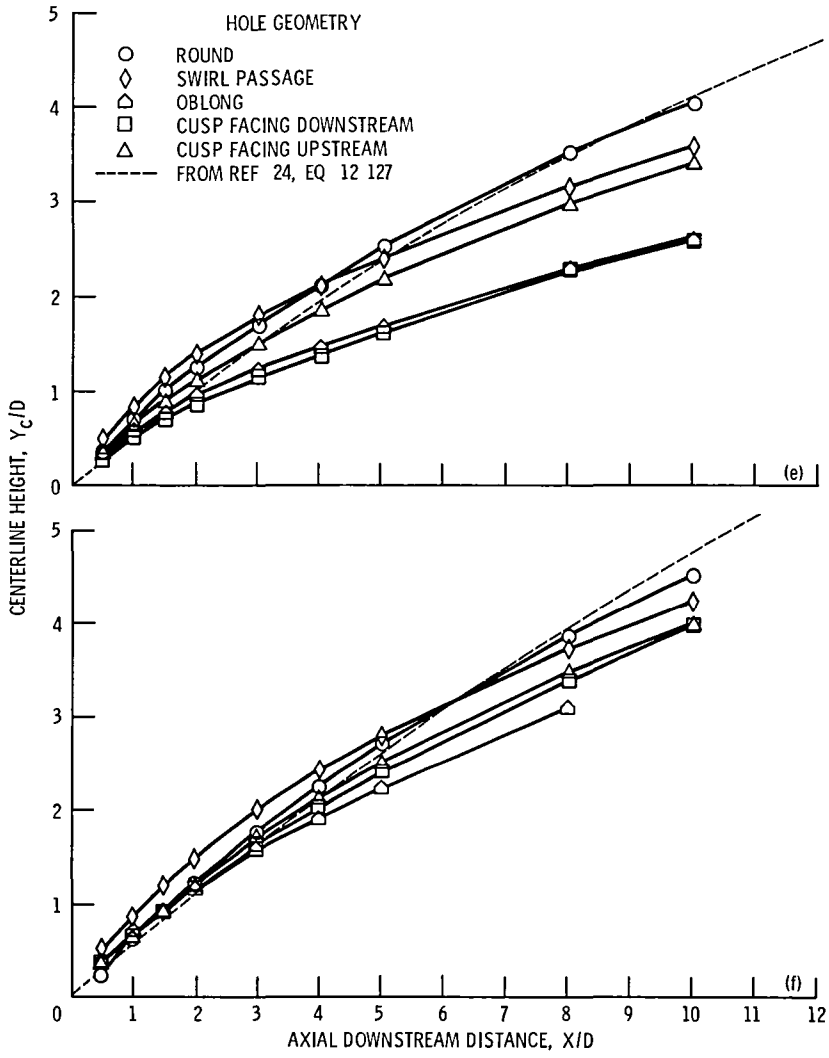

(e) M = 4.1, ρ_j/ρ_∞ = 1.03, U_∞ = 5.6 m/sec.
(f) M = 6.2, ρ_j/ρ_∞ = 1.04, U_∞ = 5.6 m/sec.

Figure 7. - Concluded.

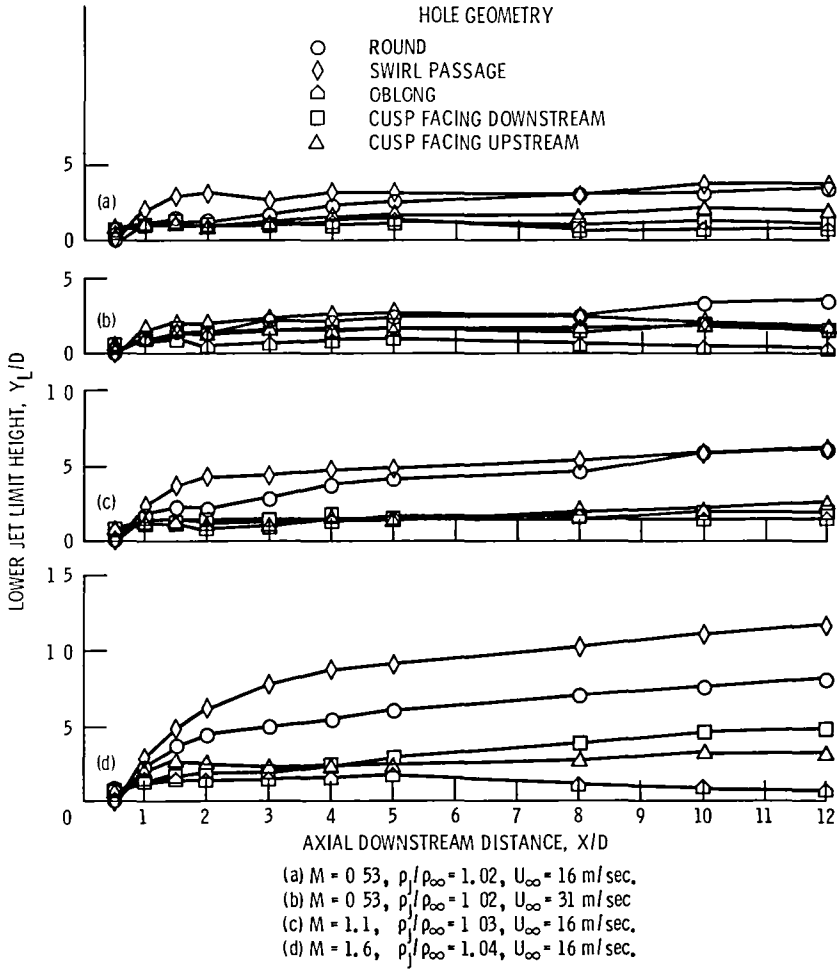

Figure 8 - Lower jet boundary height as a function of axial distance.

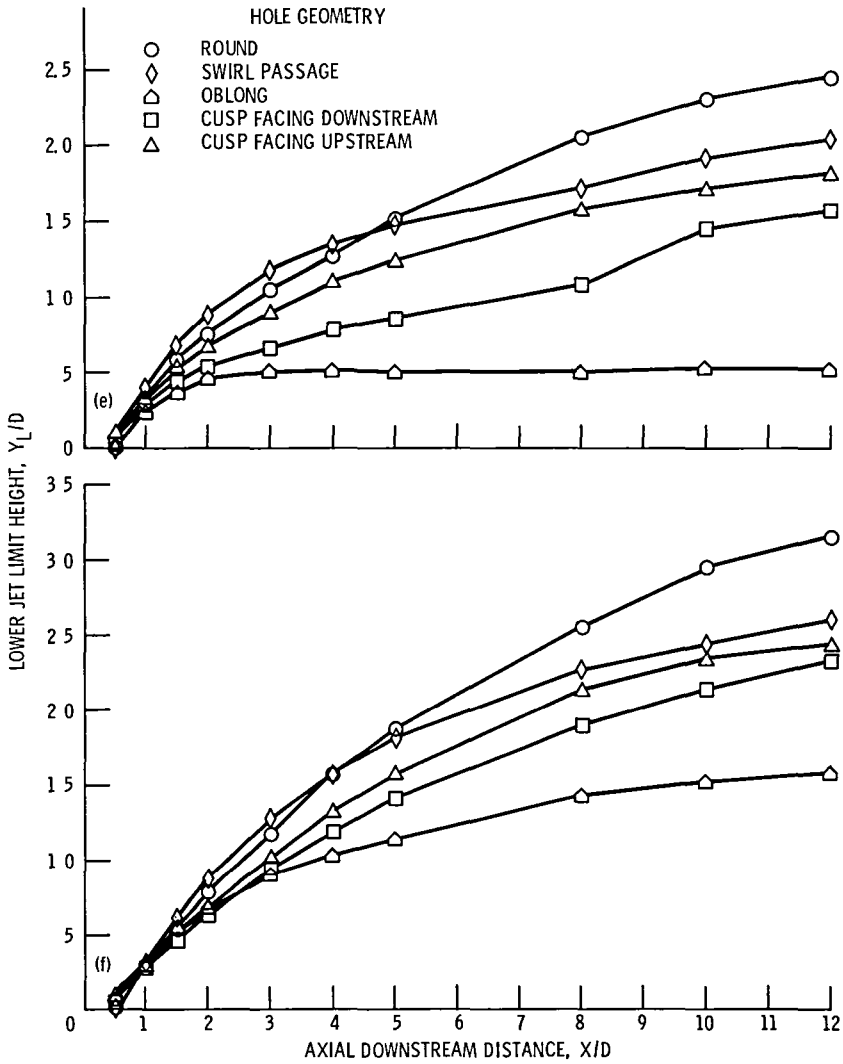

(e) M = 4.1, ρ_j/ρ_∞ = 1 03, U_∞ = 5 6 m/sec
(f) M = 6.2, ρ_j/ρ_∞ = 1 04, U_∞ = 5 6 m/sec

Figure 8. - Concluded.

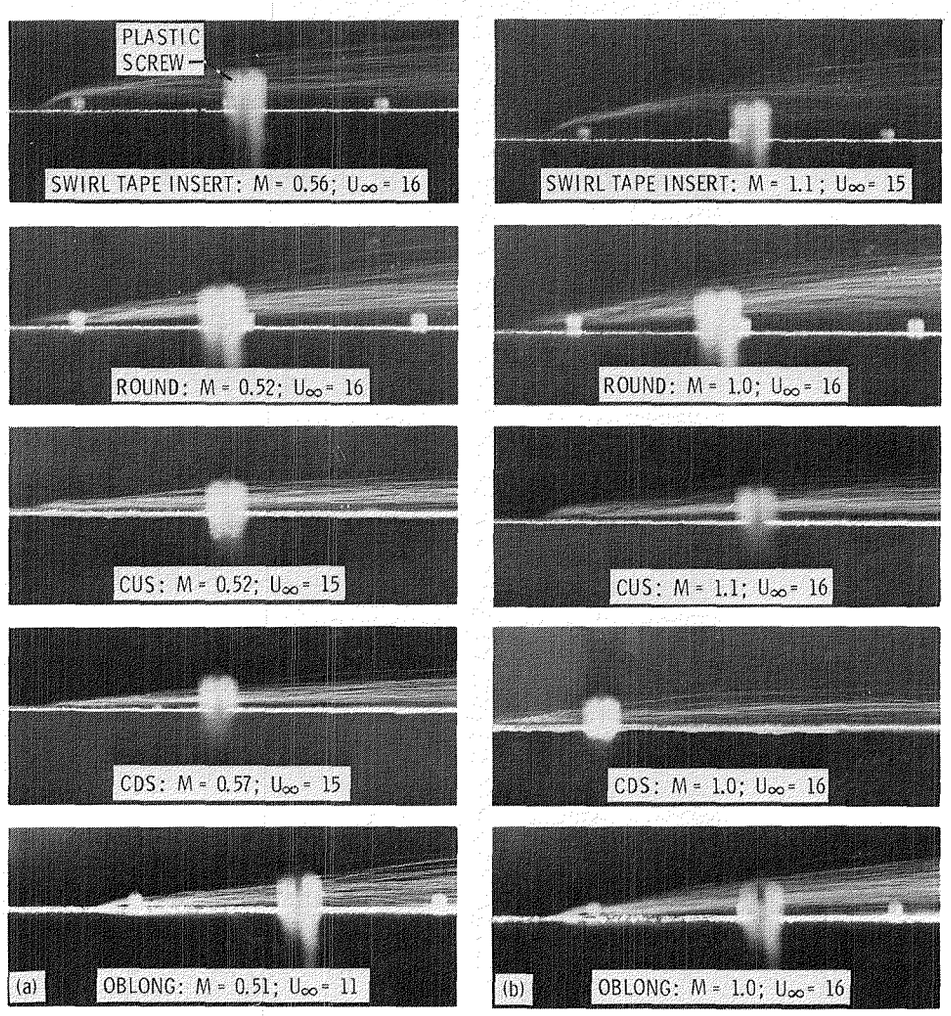

Figure 9. - Side views of jets in crossflow for various hole configurations.

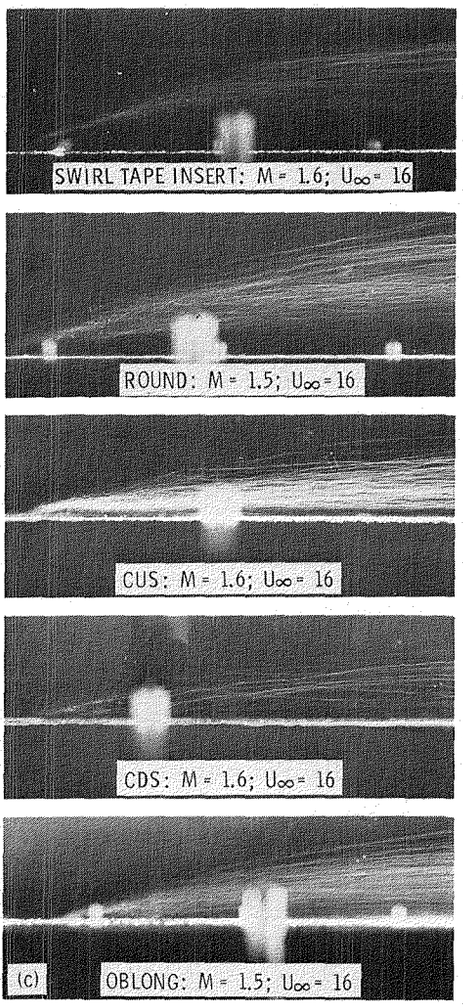

Figure 9. - Concluded.

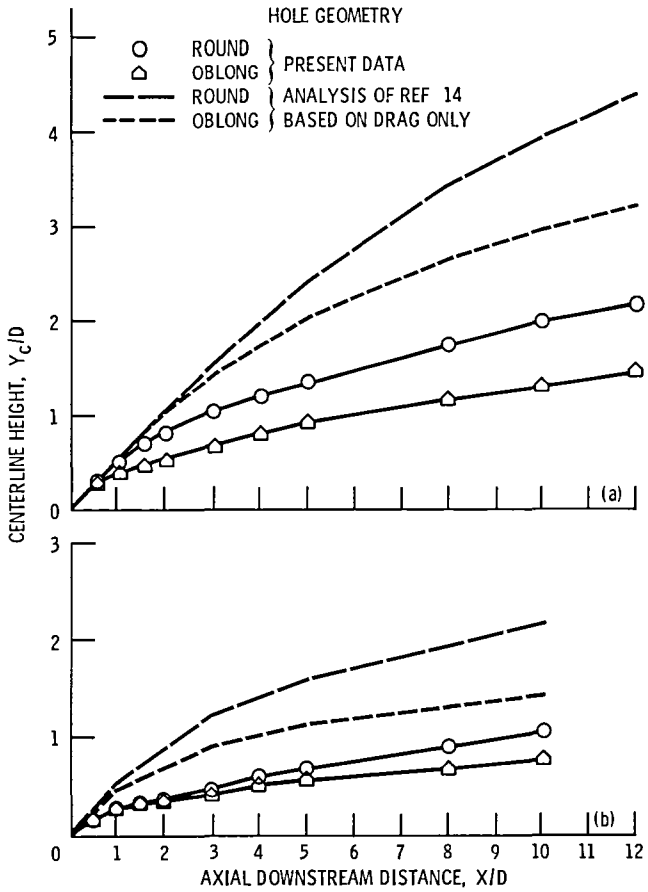

(a) M = 1 6, U_∞ = 16 m/sec
(b) M = 0 5, U_∞ = 16 m/sec

Figure 10 - Theoretical and experimental effect of drag coefficient on jet trajectory

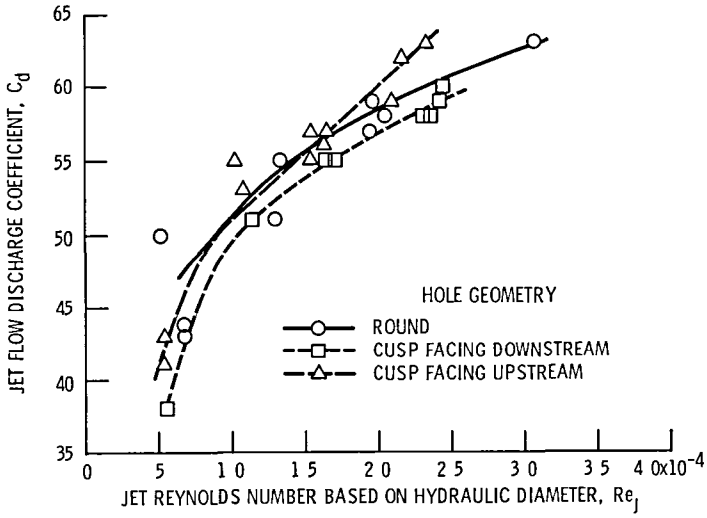

Figure 11 - Jet flow discharge coefficient as a function of jet Reynolds number

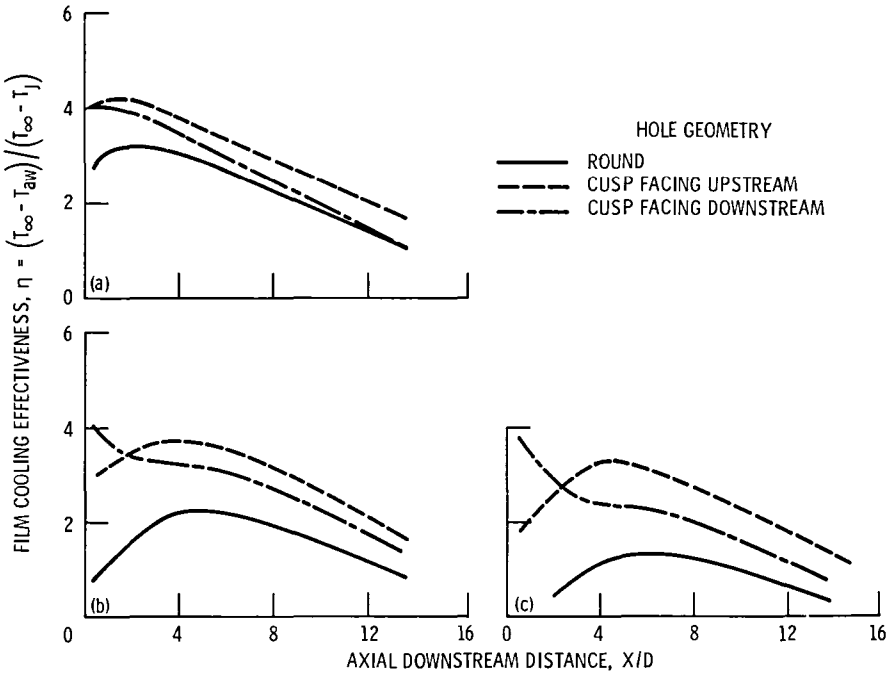

Figure 12. - Centerline film cooling effectiveness as a function of axial distance for blowing rates of 0.5, 1.0, and 1.5. Injection angle, 30°, free-stream velocity, U_∞ 15.5 m/sec. (From Ref. 1.)

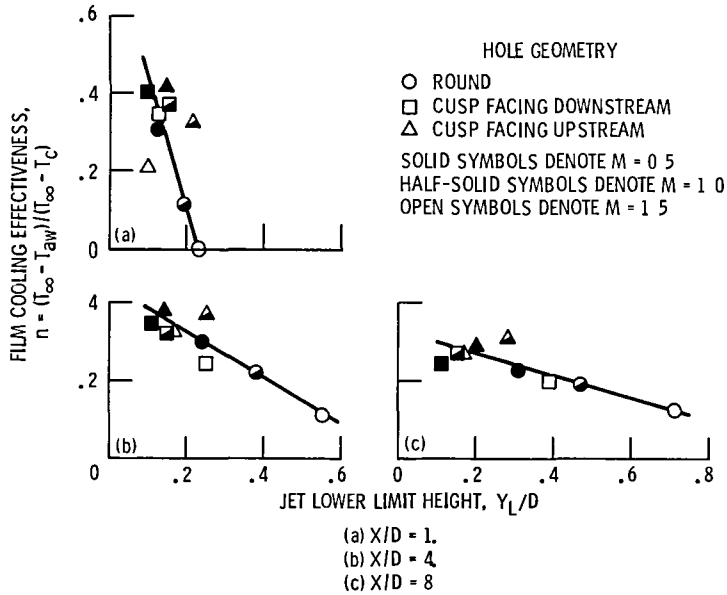

Figure 13 - Film cooling effectiveness as a function of lower jet limit height for axial distances of 1, 4, and 8.

1 Report No	2 Government Accession No	3 Recipient's Catalog No
NASA TM-86936		

4 Title and Subtitle	5 Report Date
Flow Visualization Study of the Effect of Injection Hole Geometry on an Inclined Jet in Crossflow	6 Performing Organization Code: 505-31-04

7 Author(s)	8 Performing Organization Report No
Frederick F. Simon and Michael L. Ciancone	E-2450
	10 Work Unit No

9 Performing Organization Name and Address	11 Contract or Grant No
National Aeronautics and Space Administration Lewis Research Center Cleveland, Ohio 44135	
	13 Type of Report and Period Covered: Technical Memorandum
12 Sponsoring Agency Name and Address	14 Sponsoring Agency Code
National Aeronautics and Space Administration Washington, D.C. 20546	

15 Supplementary Notes

Prepared for the Symposium on Transport Phenomena in Rotating Machinery cosponsored by the University of Michigan, University of Hawaii, ASME, Gas Turbine Society of Japan, Turbomachinery Society of Japan, and others, Honolulu, Hawaii, April 28 - May 3, 1985.

16 Abstract

A flow visualization study using neutrally buoyant, helium-filled soap bubbles was conducted to determine the effect of injection hole geometry on the trajectory of an air jet in a crossflow and to investigate the mechanisms involved in jet deflection. Experimental variables were the blowing rate (M = 0.53, 1.1, 1.6, 4.1, and 6.2) and the injection hole geometry (cusp facing upstream (CUS), cusp facing downstream (CDS), round, swirl passage, and oblong). Results indicate that jet deflection is governed by both the pressure drag forces and the entrainment of free-stream fluid into the jet flow. The effect of the pressure drag force is that a jet presenting a larger projected area to the crossflow will be deflected initially to a greater extent. Thus for injection hole geometries with similar cross-sectional areas and similar mass flow rates, the jet configuration with the larger aspect ratio (major axis perpendicular to the crossflow) experienced a greater deflection. Entrainment arises as a result of lateral shearing forces on the sides of the jet, which set up a dual vortex motion within the jet and thereby cause some of the main-stream fluid momentum to be swept into the jet flow. This additional momentum forces the jet nearer the surface. Of the jet configurations examined in this study, the oblong, CDS, and CUS configurations exhibited the largest deflections. These results correlate well with film cooling effectiveness data, suggesting the need to determine the jet exit configuration of optimum aspect ratio to provide maximum film cooling effectiveness.

17 Key Words (Suggested by Author(s))	18 Distribution Statement
Jet in crossflow; Film cooling; Hole geometry; Trajectory	Unclassified - unlimited STAR Category 34

19 Security Classif (of this report)	20 Security Classif (of this page)	21 No of pages	22 Price*
Unclassified	Unclassified		

*For sale by the National Technical Information Service, Springfield, Virginia 22161

End of Document